Available online at www.sciencedirect.com
SCIENCE DIRECT®
Journal of Computational Physics 215 (2006) 298–320
JOURNAL OF COMPUTATIONAL PHYSICS
www.elsevier.com/locate/jcp

A comparison of classical and high dimensional harmonic balance approaches for a Duffing oscillator

L. Liu *, J.P. Thomas, E.H. Dowell, P. Attar, K.C. Hall

Department of Mechanical Engineering and Materials Science, Duke University, Durham, NC 27708, USA

Received 4 April 2005; received in revised form 13 October 2005; accepted 28 October 2005
Available online 13 December 2005

Abstract

The present study focuses on a novel harmonic balance formulation, which is much easier to implement than the standard/classical harmonic balance method for complex nonlinear mathematical models and algorithms. Both harmonic balance approaches are applied to Duffing's oscillator to demonstrate the advantages and disadvantages of the two approaches. A fundamental understanding of the difference between these two methods is achieved, and the properties of each method are analyzed in detail.

MSC2000: 65P99; 74H15; 74S25

Keywords: Duffing's oscillator; Harmonic balance method; Limit cycle oscillations; Numerical analysis; Dynamical systems

1. Introduction

The harmonic balance method is a computationally efficient alternative to time marching methods for modeling nonlinear dynamic systems when the response is periodic in time. Such nonlinear dynamic systems range from models as simple as Duffing's oscillator to complex models of a complete aircraft configuration where nonlinearities may exist in both the fluid and the structure, and where flutter onset (Hopf bifurcation) and limit cycle oscillations (LCOs) are of much interest.

The classical harmonic balance (HB) approach proceeds by first substituting a temporal Fourier series expansion of the solution variables into the governing equations. Next, the equations are expanded, and the terms associated with each harmonic (i.e. $1, \cos(\omega t), \cos(2\omega t), \ldots, \cos(N_H \omega t), \sin(\omega t), \sin(2\omega t), \ldots, \sin(N_H \omega t)$) are then balanced. This yields $2N_H + 1$ equations for the $2N_H + 1$ harmonic coefficients where N_H is the number of harmonics used. The classical HB approach, especially when using only the fundamental harmonic (i.e., $N_H = 1$), which is referred to as the HB1 method in this study, has been well developed and employed successfully to study

* Corresponding author. Present address: Department of Mathematics, University of Texas Pan American, MAGC 3.210, 1201 W. University Drive, Edinburg, TX 78539, United States. Tel.: +1 919 660 5341/956 381 2578; fax: +1 919 660 0089/956 384 5091.
E-mail address: LipingLiu@utpa.edu (L. Liu).

0021-9991/$ - see front matter
doi:10.1016/j.jcp.2005.10.026

various dynamical systems. For example, Virgin [1] used the HB1 method for the Duffing's oscillator. The describing function (DF) method, similar to HB1, was employed by Shen [2] in studying the effects of a nonlinear structural spring stiffness on airfoil aeroelastic flutter and LCO behavior. The DF method was also used by Price et al. [3] to predict the nonlinear response of an airfoil with freeplay and cubic nonlinear restoring forces. The equivalent linearization method, another version of the HB1, was applied by Tang et al. [4] for an airfoil with a freeplay control surface, and by Zhao and Yang [5] to analyze the limit cycle oscillations of the airfoil. Demonstrations of the classical HB approach when including second and higher harmonics have been reported by Donescu et al. [6] for the Duffing's oscillator, and by Liu and Dowell [7,8] for a nonlinear aeroelastic airfoil model. This straightforward approach to the harmonic balance formulation is however typically difficult to implement for high dimensional nonlinear dynamical systems such as the Reynolds averaged Navier–Stokes equations for a fluid.

Recently, a new formulation of the HB method has been developed by Hall et al. [9,10] for deterministic dynamical systems, and then further developed by Beran and Pettit [11] for aeroelastic systems subject to parametric uncertainties. We denote this approach as the high dimensional harmonic balance (HDHB) method since it is suitable for high dimensional dynamical systems. The key aspect of the HDHB method is that instead of working in terms of Fourier coefficient variables as in the conventional HB approach, the dependent variables are instead cast in the time domain and stored at $2N_{\mathrm{H}}+1$ equally spaced sub-time levels over the period of one cycle of motion. The Fourier and time-domain variables are related to one another via a constant Fourier transformation matrix. Thus one might also refer to this approach as a time domain harmonic balance (TDHB) method.

Working in terms of time domain sub-time level solution variables avoids the harmonic balancing of the Fourier coefficient solution variables in the classical HB method. This makes the HDHB method very easy to formulate within the framework of an existing time marching nonlinear solver. However, the HDHB method may produce non-physical solutions as well as the physically meaningful ones that we seek. A fundamental understanding of the difference between the classical HB and HDHB approaches is needed and this is the task of the present study.

It should be mentioned that similar to the HDHB method there are some other harmonic balance approaches: the harmonic balance method (HBM) [12] and the non linear frequency domain method (NLFD) [13,14]. In these methods, the equations are set up in the frequency domain. The nonlinear terms are obtained in the time domain by using the FFT and the original differential equations. These approaches have the same advantage as the HDHB method in that no analytical expression for the nonlinear terms need to be found. However, in the HDHB method, the equations are derived and the solutions are obtained in the time domain, while in the HBM/NLFD method, one uses the FFT to convert the displacement from the frequency domain to the time domain and to convert the nonlinear terms from the time domain to the frequency domain at every iteration in the nonlinear solving process. This is more cumbersome and computationally intensive. Thus, the HDHB method is much more computationally efficient as well as more elegant than the HBM/NLFD method. Therefore, this study focuses on the comparison of the classical HB and the HDHB methods.

Duffing's oscillator [15] is a simple nonlinear scalar model that is well suited for demonstrating the differences between the two harmonic balance methods. The governing equation for Duffing's oscillator can be written as

$$m\ddot{x} + d\dot{x} + kx + \alpha x^3 = F\sin(\omega t), \tag{1}$$

where m, d, k, F and ω are the mass, damping, stiffness, external force and excitation frequency of the oscillator, respectively. Defining the natural frequency as $\omega_0 = \sqrt{k/m}$, the damping coefficient as $\zeta = d/2m\omega_0$, and non-dimensional time as $\tau = \omega_0 t$, Eq. (1) can be written as,

$$m\omega_0^2 x'' + 2\zeta\omega_0 m\omega_0 x' + \omega_0^2 mx + \alpha x^3 = F\sin\left(\frac{\omega}{\omega_0}\tau\right). \tag{2}$$

Divide both sides of the above equation by $\omega_0^2 m = k$ to obtain,

$$x'' + 2\zeta x' + x + \frac{\alpha}{k}x^3 = \frac{F}{k}\sin\left(\frac{\omega}{\omega_0}\tau\right) \tag{3}$$

Defining $h = \sqrt{k/\alpha}$, $\tilde{\omega} = \omega/\omega_0$ and the new variable $\tilde{x} = x/h$, Eq. (3) then becomes:

$$h\tilde{x}'' + 2\zeta h\tilde{x}' + h\tilde{x} + \frac{\alpha}{k}h^3\tilde{x}^3 = \frac{F}{k}\sin(\tilde{\omega}\tau)$$

Divide both sides of the above equation by h, we then have:

$$\tilde{x}'' + 2\zeta\tilde{x}' + \tilde{x} + \tilde{x}^3 = \tilde{F}\sin(\tilde{\omega}\tau) \tag{4}$$

where $\tilde{F} = F/kh = F\sqrt{\alpha}/k\sqrt{k}$. Eq. (4) is non-dimensionalized, which indicates that for any given ζ, $\tilde{\omega}$ and $\tilde{F}$, $\tilde{x}$ is a universal function of τ.

In order to identify the source of the terms in the nonlinear algebraic systems for the Fourier coefficients or the sub-time level variables, the general Duffing's equation (1) is used in Section 2. In Section 3, the non-dimensional form of the Duffing's equation (4) is used for an investigation of generic phenomena.

2. Harmonic balance analysis

Solutions periodic in time, and of a unique fundamental frequency, maybe expressed in terms of a Fourier series. The HB method consists of first substituting the Fourier expansion into the governing equations. One then integrates $R(t)g(t)$ over one period for $g(t) = \{1, \cos(\omega t), \cos(2\omega t), \ldots, \cos(N_H\omega t), \sin(\omega t), \sin(2\omega t), \ldots, \sin(N_H\omega t)\}$ where $R(t)$ is the governing equation. This provides $2N_H + 1$ equations for the $2N_H + 1$ Fourier coefficients. For a smooth $R(t)$, by using the orthogonal properties of the sine and cosine functions, this amounts to collecting terms proportional to $\cos(n\omega t)$, $n \in \{0,1,\ldots,N_H\}$ and $\sin(n\omega t)$, $n \in \{1,2,\ldots,N_H\}$.

A possible difficulty with the application of the HB technique exists for equations with non-smooth nonlinear terms. This difficulty can however be overcome using the HDHB approach. In this section, the two harmonic balance approaches are derived for Duffing's equation, and the difference between approaches is found in analytical form. Furthermore the source of the difference is also explained. We note that the HDHB method was developed for governing equations where the use of HB is not possible [9,10], such as discrete computational fluid dynamic models of the Reynolds averaged Navier–Stokes (RANS) equations. Coherent turbulence models used in RANS often contain non-smooth functions. The study of Duffing's equation allows a comparison of HB and HDHB to be made both analytically and numerically.

2.1. The standard harmonic balance method

For the derivation of the standard harmonic balance (HB) method, one begins by considering the solution of Eq. (1) to be of the form of a truncated Fourier series expansion, i.e.

$$x(t) = \hat{x}_0 + \sum_{n=1}^{N_H}(\hat{x}_{2n-1}\cos(n\omega t) + \hat{x}_{2n}\sin(n\omega t)) \tag{5}$$

Here ω is the fundamental frequency of oscillation, $\hat{x}_n (n = 0, 1, \ldots, N_H)$ are the HB solution Fourier coefficient variables, and N_H is the number of overall harmonics used in the HB truncated Fourier series expansion. The Fourier expansions of the first and second time derivative terms in Eq. (1) are

$$\begin{aligned}\dot{x}(t) &= \sum_{n=1}^{N_H}(-n\omega\hat{x}_{2n-1}\sin(n\omega t) + n\omega\hat{x}_{2n}\cos(n\omega t))\\ \ddot{x}(t) &= \sum_{n=1}^{N_H}(-(n\omega)^2\hat{x}_{2n-1}\cos(n\omega t) - (n\omega)^2\hat{x}_{2n}\sin(n\omega t)).\end{aligned} \tag{6}$$

The Fourier expansion of the cubic term in Eq. (1) may be expressed as (retaining N_H harmonics)

$$(x(t))^3 \approx \hat{r}_0 + \sum_{n=1}^{N_H}(\hat{r}_{2n-1}\cos(n\omega t) + \hat{r}_{2n}\sin(n\omega t)) \tag{7}$$

where

$$\hat{r}_0 = \frac{1}{2\pi}\int_0^{2\pi}\left(\hat{x}_0 + \sum_{n=1}^{N_H}(\hat{x}_{2n-1}\cos(nt) + \hat{x}_{2n}\sin(nt))\right)^3 \mathrm{d}t$$
$$\hat{r}_{2n-1} = \frac{1}{\pi}\int_0^{2\pi}\left(\hat{x}_0 + \sum_{n=1}^{N_H}(\hat{x}_{2n-1}\cos(nt) + \hat{x}_{2n}\sin(nt))\right)^3 \cos(nt)\,\mathrm{d}t \tag{8}$$
$$\hat{r}_{2n} = \frac{1}{\pi}\int_0^{2\pi}\left(\hat{x}_0 + \sum_{n=1}^{N_H}(\hat{x}_{2n-1}\cos(nt) + \hat{x}_{2n}\sin(nt))\right)^3 \sin(nt)\,\mathrm{d}t$$

Substituting the expressions (5)–(8) into Eq. (1) and collecting terms associated with each harmonic $\cos(n\omega t)$ and $\sin(n\omega t)$ $(n = 0,1,2,\ldots,N_H)$ yield a system of $2N_H + 1$ algebraic equations for Fourier coefficients $\hat{x}_n (n = 0,1,2,\ldots,N_H)$. The resulting algebraic system of equations can be written in vector form to determine the unknowns, $\hat{\mathbf{Q}}_x$

$$(m\omega^2\mathbf{A}^2 + d\omega\mathbf{A} + k\mathbf{I})\hat{\mathbf{Q}}_x + \alpha\hat{\mathbf{R}}_x = F\hat{\mathbf{H}} \tag{9}$$

where

$$\hat{\mathbf{Q}}_x = \begin{Bmatrix} \hat{x}_0 \\ \hat{x}_1 \\ \hat{x}_2 \\ \vdots \\ \hat{x}_{2N_H} \end{Bmatrix}_{(2N_H+1)\times 1}, \quad \hat{\mathbf{R}}_x = \begin{Bmatrix} \hat{r}_0 \\ \hat{r}_1 \\ \hat{r}_2 \\ \vdots \\ \hat{r}_{2N_H} \end{Bmatrix}_{(2N_H+1)\times 1}, \quad \hat{\mathbf{H}} = \begin{Bmatrix} 0 \\ 0 \\ 1 \\ \vdots \\ 0 \end{Bmatrix}_{(2N_H+1)\times 1}$$

and

$$\mathbf{A} = \begin{bmatrix} 0 & & & & \\ & \mathbf{J}_1 & & & \\ & & \mathbf{J}_2 & & \\ & & & \cdots & \\ & & & & \mathbf{J}_{N_H} \end{bmatrix}_{(2N_H+1)\times(2N_H+1)} \quad \text{with} \quad \mathbf{J}_n = n\begin{bmatrix} 0 & 1 \\ -1 & 0 \end{bmatrix} \; n = 1,2,\ldots,N_H.$$

Solving system (9) requires analytical expressions for the nonlinear functions $\hat{r}_i (i = 0,1,2,\ldots,2N_H)$ in terms of the variables $\hat{x}_i (i = 0,1,2,\ldots,2N_H)$.

For HB1, i.e. $N_H = 1$, Eq. (9) can be written as

$$\begin{aligned} &(k + \alpha(A_0^2 + \frac{3}{2}A_1^2))\hat{x}_0 = 0 \\ &(k - m\omega^2)\hat{x}_1 + d\omega\hat{x}_2 + \alpha(3A_0^2 + \frac{3}{4}A_1^2)\hat{x}_1 = 0 \\ &-d\omega\hat{x}_1 + (k - m\omega^2)\hat{x}_2 + \alpha(3A_0^2 + \frac{3}{4}A_1^2)\hat{x}_2 = F \end{aligned} \tag{10}$$

where $A_0 \equiv \sqrt{\hat{x}_0^2}$ and $A_1 \equiv \sqrt{\hat{x}_1^2 + \hat{x}_2^2}$. For the linear case ($\alpha = 0$), the solution to Eq. (9) is $\hat{x}_0 = 0$, $\hat{x}_1 = -\frac{Fd\omega}{(k-m\omega^2)^2+(d\omega)^2}$, and $\hat{x}_2 = \frac{F(k-m\omega^2)}{(k-m\omega^2)^2+(d\omega)^2}$, which turns out to be the exact solution for the steady state motion.

For the nonlinear case, this study focuses on the hardening spring: $k > 0$ and $\alpha > 0$. From the first equation of system (10), $\hat{x}_0 = 0$. An analytical solutions for $\hat{x}_1$ and $\hat{x}_2$ cannot be obtained. However, the amplitude (A_1) frequency (ω) relationship is

$$((d\omega)^2 + (k - m\omega^2 + \alpha\frac{3}{4}A_1^2)^2)A_1^2 = F^2 \tag{11}$$

This is a third degree polynomial in A_1^2, and thus there are three possible solutions for the amplitude. Real valued amplitudes are the only solutions which are physically meaningful. More detailed results are presented in the next section.

When the nonlinearity is strong, the solution may not be strictly harmonic. Also higher harmonics may significantly contribute to the overall solution. Moreover, when many harmonics are included in the analysis the resulting expression from Eq. (8) may be long and complex.

2.2. The high dimensional harmonic balance method

For a model where the nonlinearity in the governing equations is a simple polynomial function of the solution variables (e.g. Duffing's equation (1)), the standard HB approach is typically easy to implement. However, for models with more complex nonlinearities, it may be very difficult or impossible to implement the standard HB approach. Furthermore, if the governing model is based upon some existing computational model, when using the standard HB approach, it is always then necessary to write a separate and different computational code. The recently developed HDHB approach (e.g. [9,10]) overcomes these difficulties. The HDHB procedure for Duffing's oscillator is outlined in the following.

The $(2N_H + 1)$ harmonic balance Fourier coefficient solution variables are related to the time domain solution at $2N_H + 1$ equally spaced sub-time levels over a period of oscillation via a constant Fourier transformation matrix. That is

$$\hat{\mathbf{Q}}_x = \mathbf{E}\tilde{\mathbf{Q}}_x, \tag{12}$$

where

$$\tilde{\mathbf{Q}}_x = \begin{Bmatrix} x(t_0) \\ x(t_1) \\ x(t_2) \\ \vdots \\ x(t_{2N_H}) \end{Bmatrix},$$

with $t_i = \frac{i2\pi}{2N_H+1} (i = 0, 1, 2, \ldots, 2N_H)$, and the transform matrix is

$$\mathbf{E} = \frac{2}{2N_H + 1} \begin{bmatrix} 1/2 & 1/2 & ... & 1/2 \\ \cos t_0 & \cos t_1 & \ldots & \cos t_{2N_H} \\ \sin t_0 & \sin t_1 & \ldots & \sin t_{2N_H} \\ \cos 2t_0 & \cos 2t_1 & \ldots & \cos 2t_{2N_H} \\ \sin 2t_0 & \sin 2t_1 & \ldots & \sin 2t_{2N_H} \\ \vdots & \vdots & & \vdots \\ \cos N_H t_0 & \cos N_H t_1 & \ldots & \cos N_H t_{2N_H} \\ \sin N_H t_0 & \sin N_H t_1 & \ldots & \sin N_H t_{2N_H} \end{bmatrix}.$$

Furthermore, the time domain solutions at the $2N_H + 1$ equally spaced sub-time levels can be expressed in terms of the harmonic balance Fourier coefficients solution using the inverse of the Fourier transformation matrix, i.e.

$$\tilde{\mathbf{Q}}_x = \mathbf{E}^{-1}\hat{\mathbf{Q}}_x, \tag{13}$$

where

$$\mathbf{E}^{-1} = \begin{bmatrix} 1 & \cos t_0 & \sin t_0 & \ldots & \cos N_H t_0 & \sin N_H t_0 \\ 1 & \cos t_1 & \sin t_1 & \ldots & \cos N_H t_1 & \sin N_H t_1 \\ \vdots & \vdots & \vdots & & \vdots & \vdots \\ 1 & \cos t_{2N_H} & \sin t_{2N_H} & \ldots & \cos N_H t_{2N_H} & \sin N_H t_{2N_H} \end{bmatrix}$$

Similarly $\hat{\mathbf{R}}_x = \mathbf{E}\tilde{\mathbf{R}}_x$ and $\hat{\mathbf{H}} = \mathbf{E}\tilde{\mathbf{H}}$, where

$$\tilde{\mathbf{R}}_x = \begin{Bmatrix} x(t_0)^3 \\ x(t_1)^3 \\ \vdots \\ x(t_{2N_H})^3, \end{Bmatrix} \quad \tilde{\mathbf{H}} = \begin{Bmatrix} \sin t_0 \\ \sin t_1 \\ \vdots \\ \sin t_{2N_H} \end{Bmatrix}.$$

Eq. (9) is then rewritten as

$$(m\omega^2\mathbf{A}^2 + d\omega\mathbf{A} + k\mathbf{I})\mathbf{E}\tilde{\mathbf{Q}}_x + \alpha\mathbf{E}\tilde{\mathbf{R}}_x = F\mathbf{E}\tilde{\mathbf{H}} \tag{14}$$

Multiplying both sides of Eq. (14) by $\mathbf{E}^{-1}$ gives:

$$(m\omega^2\mathbf{D}^2 + d\omega\mathbf{D} + k\mathbf{I})\tilde{\mathbf{Q}}_x + \alpha\tilde{\mathbf{R}}_x = F\tilde{\mathbf{H}} \tag{15}$$

where $\mathbf{D} = \mathbf{E}^{-1}\mathbf{A}\mathbf{E}$. In this study, the above system is referred as the HDHB solution system.

Solving Eq. (15) does not require any analytical expressions for the Fourier components. Also, it is easy to implement the HDHB system into an existing time marching code, e.g. a time marching computational fluid dynamics (CFD) code. The main requirement for implementing the HDHB method is a re-dimensioning of the primary arrays from N elements to $N \times (2N_H + 1)$ elements, while the rest of the flow solver remains relatively unchanged.

2.3. Differences between the HB and HDHB methods

In order to explore the difference between the HB and HDHB methods, Eq. (15) is expressed in terms of frequency domain variables. From Eq. (12), $x(t_i)$ $(i = 0,1,2,\ldots,2N_H)$ is the $(i+1)$th component of the vector $\mathbf{E}^{-1}\hat{\mathbf{Q}}_x, x(t_i) = (\mathbf{E}^{-1}\hat{\mathbf{Q}}_x)|_{i+1}$. The nonlinear term in Eq. (15) is

$$\tilde{\mathbf{R}}_x = \begin{Bmatrix} \left(|\mathbf{E}^{-1}\hat{\mathbf{Q}}_x|_1\right)^3 \\ \left(|\mathbf{E}^{-1}\hat{\mathbf{Q}}_x|_2\right)^3 \\ \vdots \\ \left(|\mathbf{E}^{-1}\hat{\mathbf{Q}}_x|_{2N_H+1}\right)^3 \end{Bmatrix} \equiv \left(\mathbf{E}^{-1}\hat{\mathbf{Q}}_x\right)^3 \tag{16}$$

Here a vector's cubic power is defined as the vector of the cubic power of each component. With (16) and (12), Eq. (15) becomes

$$(m\omega^2\mathbf{D}^2 + d\omega\mathbf{D} + k\mathbf{I})\mathbf{E}^{-1}\hat{\mathbf{Q}}_x + \alpha(\mathbf{E}^{-1}\hat{\mathbf{Q}}_x)^3 = F\mathbf{E}^{-1}\hat{\mathbf{H}} \tag{17}$$

Multiplying both sides of (17) by $\mathbf{E}$ yields the equivalent system of (15) in the frequency domain:

$$(m\omega^2\mathbf{A}^2 + d\omega\mathbf{A} + k\mathbf{I})\hat{\mathbf{Q}}_x + \alpha\mathbf{E}(\mathbf{E}^{-1}\hat{\mathbf{Q}}_x)^3 = F\hat{\mathbf{H}} \tag{18}$$

From (9) and (18), the difference between the HB and HDHB systems is really the difference between $\hat{\mathbf{R}}_x$, whose elements are defined in (8), and $\mathbf{E}(\mathbf{E}^{-1}\hat{\mathbf{Q}}_x)^3$. Without loss of generality, denote

$$\mathbf{E}(\mathbf{E}^{-1}\hat{\mathbf{Q}}_x)^3 \equiv \hat{\mathbf{P}}_x = \begin{Bmatrix} \hat{p}_0 \\ \hat{p}_1 \\ \vdots \\ \hat{p}_{2N_H} \end{Bmatrix}. \tag{19}$$

For $N_H = 1$, from (10) or (7) in the HB approach, the Fourier components for the cubic function are

$$\hat{\mathbf{R}}_x = \begin{Bmatrix} (A_0^2 + \frac{3}{2}A_1^2)\hat{x}_0 \\ (3A_0^2 + \frac{3}{4}A_1^2)\hat{x}_1 \\ (3A_0^2 + \frac{3}{4}A_1^2)\hat{x}_2 \end{Bmatrix} \tag{20}$$

From (19) in the HDHB approach, the Fourier components for the cubic function are

$$\hat{\mathbf{P}}_x = \begin{Bmatrix} (A_0^2 + \frac{3}{2}A_1^2)\hat{x}_0 + \frac{1}{4}\hat{x}_1^3 - \frac{3}{4}\hat{x}_1\hat{x}_2^2 \\ (3A_0^2 + \frac{3}{4}A_1^2)\hat{x}_1 + \frac{3}{2}\bar{A}_1^2\hat{x}_0 \\ (3A_0^2 + \frac{3}{4}A_1^2)\hat{x}_2 - 3\hat{x}_0\hat{x}_1\hat{x}_2 \end{Bmatrix} = \begin{Bmatrix} \hat{r}_0 + \frac{1}{4}\hat{x}_1^3 - \frac{3}{4}\hat{x}_1\hat{x}_2^2 \\ \hat{r}_1 + \frac{3}{2}\bar{A}_1^2\hat{x}_0 \\ \hat{r}_2 - 3\hat{x}_0\hat{x}_1\hat{x}_2 \end{Bmatrix} \tag{21}$$

where $\bar{A}_1 = \sqrt{\hat{x}_1^2 - \hat{x}_2^2}$, and $\hat{r}_i (i = 0, 1, 2)$ in (21) is the $(i+1)$th component in $\hat{\mathbf{R}}_x$ in (20). Furthermore, system (18) in explicit form becomes

$$\begin{aligned} &k\hat{x}_0 + \alpha\left(\left(A_0^2 + \frac{3}{2}A_1^2\right)\hat{x}_0 + \frac{1}{4}\hat{x}_1^3 - \frac{3}{4}\hat{x}_1\hat{x}_2^2\right) = 0 \\ &(k - m\omega^2)\hat{x}_1 + d\omega\hat{x}_2 + \alpha\left(\left(3A_0^2 + \frac{3}{4}A_1^2\right)\hat{x}_1 + \frac{3}{2}\bar{A}_1^2\hat{x}_0\right) = 0 \\ &-d\omega\hat{x}_1 + (k - m\omega^2)\hat{x}_2 + \alpha\left(\left(3A_0^2 + \frac{3}{4}A_1^2\right)\hat{x}_2 - 3\hat{x}_0\hat{x}_1\hat{x}_2\right) = F \end{aligned} \tag{22}$$

Comparing (22) with (10), the HDHB1 system (22) contains all the terms that appear in the HB1 system (10) *plus* some additional terms.

Similarly, for $N_H = 2$, the Fourier components in the HB method for the cubic function are

$$\hat{\mathbf{R}}_x = \begin{Bmatrix} A_0^2\hat{x}_0 + \frac{3}{2}A_1^2\hat{x}_0 + \frac{3}{2}A_2^2\hat{x}_0 + \frac{3}{4}\bar{A}_1^2\hat{x}_3 + \frac{3}{2}\hat{x}_1\hat{x}_2\hat{x}_4 \\ 3A_0^2\hat{x}_1 + \frac{3}{4}A_1^2\hat{x}_1 + \frac{3}{2}A_2^2\hat{x}_1 + 3\hat{x}_0\hat{x}_1\hat{x}_3 + 3\hat{x}_0\hat{x}_2\hat{x}_4 \\ 3A_0^2\hat{x}_2 + \frac{3}{4}A_1^2\hat{x}_2 + \frac{3}{2}A_2^2\hat{x}_2 + 3\hat{x}_0\hat{x}_1\hat{x}_4 - 3\hat{x}_0\hat{x}_2\hat{x}_3 \\ 3A_0^2\hat{x}_3 + \frac{3}{2}A_1^2\hat{x}_3 + \frac{3}{4}A_2^2\hat{x}_3 + \frac{3}{2}\bar{A}_1^2\hat{x}_0 \\ 3A_0^2\hat{x}_4 + \frac{3}{2}A_1^2\hat{x}_4 + \frac{3}{4}A_2^2\hat{x}_4 + 3\hat{x}_0\hat{x}_1\hat{x}_2 \end{Bmatrix} \tag{23}$$

while in the HDHB approach, the Fourier components for the cubic function are

$$\hat{\mathbf{P}}_x = \begin{Bmatrix} \hat{r}_0 + \frac{3}{4}\bar{A}_2^2\hat{x}_1 - \frac{3}{2}\hat{x}_2\hat{x}_3\hat{x}_4 \\ \hat{r}_1 + \frac{3}{4}\bar{A}_1^2\hat{x}_3 + \frac{3}{2}\bar{A}_2^2\hat{x}_0 + \frac{1}{4}\hat{x}_3^3 - \frac{3}{4}\hat{x}_3\hat{x}_4^2 - \frac{3}{2}\hat{x}_1\hat{x}_2\hat{x}_4 \\ \hat{r}_2 - \frac{3}{4}\bar{A}_1^2\hat{x}_4 - \frac{1}{4}\hat{x}_4^3 + \frac{3}{4}\hat{x}_3^2\hat{x}_4 - \frac{3}{2}\hat{x}_1\hat{x}_2\hat{x}_3 - 3\hat{x}_0\hat{x}_3\hat{x}_4 \\ \hat{r}_3 + \frac{1}{4}\hat{x}_1^3 + \frac{3}{4}\bar{A}_2^2\hat{x}_1 - \frac{3}{4}\hat{x}_1\hat{x}_2^2 + \frac{3}{2}\hat{x}_2\hat{x}_3\hat{x}_4 + 3\hat{x}_0\hat{x}_1\hat{x}_3 - 3\hat{x}_0\hat{x}_2\hat{x}_4 \\ \hat{r}_4 + \frac{1}{4}\hat{x}_2^3 + \frac{3}{4}\bar{A}_2^2\hat{x}_2 - \frac{3}{4}\hat{x}_1^2\hat{x}_2 - \frac{3}{2}\hat{x}_1\hat{x}_3\hat{x}_4 - 3\hat{x}_0\hat{x}_2\hat{x}_3 - 3\hat{x}_0\hat{x}_1\hat{x}_4 \end{Bmatrix} \tag{24}$$

where $A_2 = \sqrt{\hat{x}_3^2 + \hat{x}_4^2}$, $\bar{A}_2 = \sqrt{\hat{x}_3^2 - \hat{x}_4^2}$, and $\hat{r}_i (i = 0, 1, 2, 3, 4)$ in (24) is the $(i+1)$th component in $\hat{\mathbf{R}}_x$ in (23). Therefore, again, the HDHB2 system retains all the terms in HB2 system *plus* some additional terms.

Further study of the HB and HDHB solution systems reveals that the HDHB system always contains more terms than the HB system when using the same number of harmonics for all higher order harmonic approximations.

As discussed in the following section, the additional terms in the HDHB system admits more solutions than the HB system. Therefore, it is interesting and valuable to determine the source of these terms. In the HB approach, the assumed harmonic motion form is substituted in the differential system (1), and the Fourier components of each term ($m\ddot{x}, d\dot{x}, kx, \alpha x^3$ and $F\sin\omega t$) are obtained. Furthermore, the same number of harmonics are kept in the HB system for each term in the original governing equation. On the other hand, in the HDHB approach, when the assumed harmonic motion form is substituted in (1), the individual harmonics

are not specifically obtained. For the linear terms (linear with respect to $x : m\ddot{x}, d\dot{x}, kx$ and $F\sin\omega t$), the HDHB method produces the same result as the HB method does as the order of the harmonics does not change after the linear operators. Therefore, the source of any difference is related to the nonlinear term x^3.

To illustrate, consider $N_H = 1$, and a solution of the form

$$x(t) = \hat{x}_0 + \hat{x}_1\cos\omega t + \hat{x}_2\sin\omega t.$$

When expanded, the nonlinear term $x(t)^3$ is

$$\begin{aligned}(x(t))^3 &= (\hat{x}_0 + \hat{x}_1\cos\omega t + \hat{x}_2\sin\omega t)^3\\ &= \left(A_0^2 + \frac{3}{4}A_1^2\right)\hat{x}_0 + \left(3A_0^2 + \frac{3}{4}A_1^2\right)\hat{x}_1\cos\omega t + \left(3A_0^2 + \frac{3}{4}A_1^2\right)\hat{x}_2\sin\omega t\\ &\quad + \frac{3}{2}\bar{A}_1^2\hat{x}_0\cos 2\omega t + 3\hat{x}_0\hat{x}_1\hat{x}_2\sin 2\omega t + \frac{1}{4}\left(-3\hat{x}_2^2 + \hat{x}_1^2\right)\hat{x}_1\cos 3\omega t + \frac{1}{4}\left(3\hat{x}_1^2 - \hat{x}_2^2\right)\hat{x}_2\sin 3\omega t\end{aligned} \tag{25}$$

The HB1 method retains the coefficients of the zeroth and the first harmonics, i.e. the coefficients of 1, $\cos\omega t$ and $\sin\omega t$, and disregards the higher order harmonics. On the other hand, the HDHB1 system retains every term in (25), including the harmonics that are higher than the first harmonic, i.e., including the coefficients of $\cos 2\omega t$, $\sin 2\omega t$, $\cos 3\omega t$ and $\sin 3\omega t$. The coefficients of the higher order harmonics associated with 2ω and 3ω are absorbed in the HDHB1 system by the transform matrix $\mathbf{E}$: the coefficient of $\cos 2\omega t$ appears in $\hat{p}_1$, the coefficient of $\sin 2\omega t$ appears in $\hat{p}_2$, the coefficient of $\cos 3\omega t$ appears in $\hat{p}_0$, the coefficient of $\sin 3\omega t$ is multiplied by zero and disappears in $\hat{\mathbf{P}}_x$.

Similarly, when $N_H = 2$, the solution form and the nonlinear term become

$$x(t) = \hat{x}_0 + \hat{x}_1\cos\omega t + \hat{x}_2\sin\omega t + \hat{x}_3\cos 2\omega t + \hat{x}_4\sin 2\omega t,$$

and

$$\begin{aligned}(x(t))^3 &= (\hat{x}_0 + \hat{x}_1\cos\omega t + \hat{x}_2\sin\omega t + \hat{x}_3\cos 2\omega t + \hat{x}_4\sin 2\omega t)^3\\ &= \hat{r}_0 + \hat{r}_1\cos\omega t + \hat{r}_2\sin\omega t + \hat{r}_3\cos 2\omega t + \hat{r}_4\sin 2\omega t\\ &\quad + \left(-\frac{3}{4}\hat{x}_2^2\hat{x}_1 + \frac{1}{4}\hat{x}_1^3 + \frac{2}{3}\hat{x}_2\hat{x}_3\hat{x}_4 - 3\hat{x}_0\hat{x}_2\hat{x}_4 + 3\hat{x}_0\hat{x}_1\hat{x}_2 + \frac{3}{4}\bar{A}_2^2\hat{x}_1\right)\cos 3\omega t\\ &\quad + \left(\frac{3}{4}\hat{x}_1^2\hat{x}_2 - \frac{1}{4}\hat{x}_2^3 - \frac{3}{4}\bar{A}_2^2\hat{x}_2 + 3\hat{x}_0\hat{x}_1\hat{x}_4 + 3\hat{x}_0\hat{x}_2\hat{x}_3 + \frac{3}{2}\hat{x}_1\hat{x}_3\hat{x}_4\right)\sin 3\omega t\\ &\quad + \left(-\frac{3}{2}\hat{x}_1\hat{x}_2\hat{x}_4 + \frac{3}{2}\bar{A}_2^2\hat{x}_0 + \frac{3}{4}\bar{A}_1^2\hat{x}_3\right)\cos 4\omega t + \left(\frac{3}{2}\hat{x}_1\hat{x}_2\hat{x}_3 + 3\hat{x}_0\hat{x}_3\hat{x}_4 + \frac{3}{4}\bar{A}_1^2\hat{x}_4\right)\sin 4\omega t\\ &\quad + \left(-\frac{3}{2}\hat{x}_2\hat{x}_3\hat{x}_4 + \frac{3}{4}\bar{A}_2^2\hat{x}_1\right)\cos 5\omega t + \left(\frac{3}{2}\hat{x}_1\hat{x}_3\hat{x}_4 + \frac{3}{4}\bar{A}_2^2\hat{x}_2\right)\sin 5\omega t + \left(\frac{1}{4}\hat{x}_3^3 - \frac{3}{4}\hat{x}_3\hat{x}_4^2\right)\cos 6\omega t\\ &\quad + \left(\frac{3}{4}\hat{x}_3^2\hat{x}_4 - \frac{1}{4}\hat{x}_4^3\right)\sin 6\omega t.\end{aligned} \tag{26}$$

The coefficients of all harmonics in (26) can be identified in (24): the coefficient of $\cos 3\omega t$ is absorbed in $\hat{p}_0$ and $\hat{p}_3$; the coefficient of $\sin 3\omega t$ appears in $\hat{p}_4$ (some of the terms disappear and may not show in $\hat{\mathbf{P}}_x$); the coefficient of $\cos 4\omega t$ appears in $\hat{p}_1$; the coefficient of $\sin 4\omega t$ appears in $\hat{p}_2$; the coefficient of $\cos 5\omega t$ appears in $\hat{p}_3$; the coefficient of $\sin 5\omega t$ appears in $\hat{p}_4$; the coefficient of $\cos 6\omega t$ appears in $\hat{p}_1$; and the coefficient of $\sin 6\omega t$ appears in $\hat{p}_2$.

Generally, using the ansatz (5), the truncated Fourier expansion for the nonlinear function is used in the HB approach, i.e. (7) is used in system (9), while the whole Fourier expansion for the nonlinear function is used in the HDHB approach:

$$(x(t))^3 = \hat{r}_0 + \sum_{n=1}^{N_H}(\hat{r}_{2n-1}\cos n\omega t + \hat{r}_{2n}\sin n\omega t) + \sum_{n=N_H+1}^{\infty}(\hat{r}_{2n-1}\cos n\omega t + \hat{r}_{2n}\sin n\omega t) \tag{27}$$

For sufficiently small amplitudes, the HDHB results are close to the HB results while for large amplitudes or motions with many dominant high harmonics, the extra terms in the HDHB system may become significant

and cause significant difference between the HDHB and the HB results for any fixed N_H. However, when N_H approaches to infinity, (7) and (27) are essentially identical, therefore, these two approaches are asymptotically equivalent.

3. Results and discussions

For linear systems, the HB and HDHB approaches are equivalent, however, as shown in the Section 2.3, when a nonlinear term is present, the results from the HB and HDHB methods are different. In the following discussion, the universal form (4) of the Duffing's oscillator is used. For simplification, the ~ is subsequently omitted in the results to be shown in this section. Without loss of generality, the damping is chosen as $\zeta = 0.1$. Depending on the hysteresis branch in the amplitude-frequency relationship curve, the results from the HB and HDHB approaches vary. The representative cases chosen for illustration in the following discussion correspond to 'no hysteresis' ($F = 0.025$), 'small region of hysteresis' ($F = 0.25$) and 'large region of hysteresis' ($F = 1.25$).

3.1. Weak nonlinearity resulting in no hysteresis

Shown in Fig. 1 are the computed zeroth ($A_0 = |\hat{x}_0|$) and first harmonic ($A_1 = \sqrt{\hat{x}_1^2 + \hat{x}_2^2}$) amplitudes for the case of $F = 0.025$ when using the time marching method (e.g., Runge–Kutta scheme) in addition to results obtained via the standard harmonic balance (HB) and high dimensional harmonic balance (HDHB) methods using one harmonic. The results for the three different methods can be seen to be essentially identical. For small external forces when no hysteresis is present in the solution, the zeroth harmonic amplitude is zero ($A_0 = 0$, i.e. $\hat{x}_0 = 0$), which means (recall Eqs. (10) and (22)) that the HB1 and HDHB1 systems yield identical results.

3.2. Nonlinearity resulting in a small region of hysteresis

3.2.1. Time marching results

We next consider the case of $F = 0.25$, which results in a small region of hysteresis in the solution. Shown in Fig. 2 are time marching solutions for the peak response amplitude as a function of the excitation frequency. The open circles represent the solution when gradually increasing the frequency from a starting value of 0.05, and the dots represent the solution when decreasing the frequency from a starting value of 2.5. As can be seen,

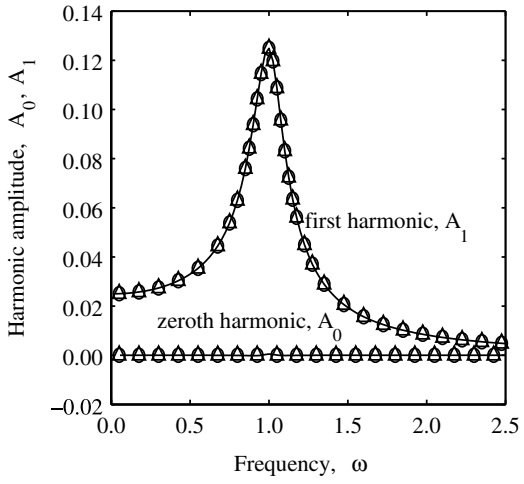

Fig. 1. Comparison of the results from time marching, HB and HDHB methods, $F = 0.025$. Solid line: time marching; triangle: HB; circle: HDHB.

a small region of hysteresis is present between the frequencies of $\omega \approx 1.270$ and $\omega \approx 1.325$. Fig. 2(b) shows a close-up of the region of hysteresis. From Fig. 2, it can be seen that there is also a small region of slightly increased peak response amplitude for frequency near $\omega = 0.375$. A frequency domain analysis of the time marching solution reveals that the solution near this frequency of excitation consists of not only a component corresponding to the fundamental harmonic, but also higher order harmonic components.

3.2.2. Harmonic balance results

For the standard HB method, depending on the starting frequency and initial condition for the Newton–Raphson (NR) solver, two slightly different sets of results are obtained. Nonetheless, the amplitudes of the zeroth harmonic A_0, and the eventh order harmonics (A_2, A_4, ...) of the solution are always zero, which is in an agreement with the time marching solution.

Similar to the procedure for computing the time marching solution in Fig. 2, an initial excitation frequency is chosen, low or high (say 0.05 or 2.50), and a solution for Duffing's equation is computed (in this case we simply use $X = 0$ as an initial condition). Next, we either slightly increase the excitation frequency (when starting from a low frequency), or slightly decrease the excitation frequency (when starting from a high frequency), and use the solution from the previous computation as an initial condition for the HB solution process. A peak amplitude response similar to Fig. 2 can be constructed from the HB method.

As shown in Eq. (11), the solution of the standard harmonic balance method when using one harmonic (HB1) is a root of a third order polynomial equation. Three solutions are possible, but it is the purely real valued solutions for A_1 that are physically meaningful. For the low frequency (lower than 1.27), there are one real root and one pair of conjugate complex roots. But only the real root is a physically meaningful solution for A_1. For the frequencies between 1.27 and 1.325, there are three real roots, and therefore these three roots are physically meaningful solutions. For the high frequency (higher than 1.325), similar to the case of low frequency, there are one real root and one pair of conjugate complex roots from Eq. (11). Within the hysteresis frequency range $\omega \in [1.270, 1.325]$, the HB1 method is capable of predicting all three of the possible solution amplitudes. The solution obtained depends on the chosen initial condition.

The solution determination process when using more than one harmonic for the standard harmonic balance method follows the same procedure as when using just one harmonic. Solutions from lower number of harmonic analysis can be used as initial conditions. The higher harmonic components are simply set to zero for the initial condition. We again note that the unstable branch of the solution to Duffing's equation cannot be predicted using conventional time marching methods. Of course, one could find the unstable branch by using other time marching methods, e.g. the shooting with arc-length continuation method [16]. Fig. 3 shows

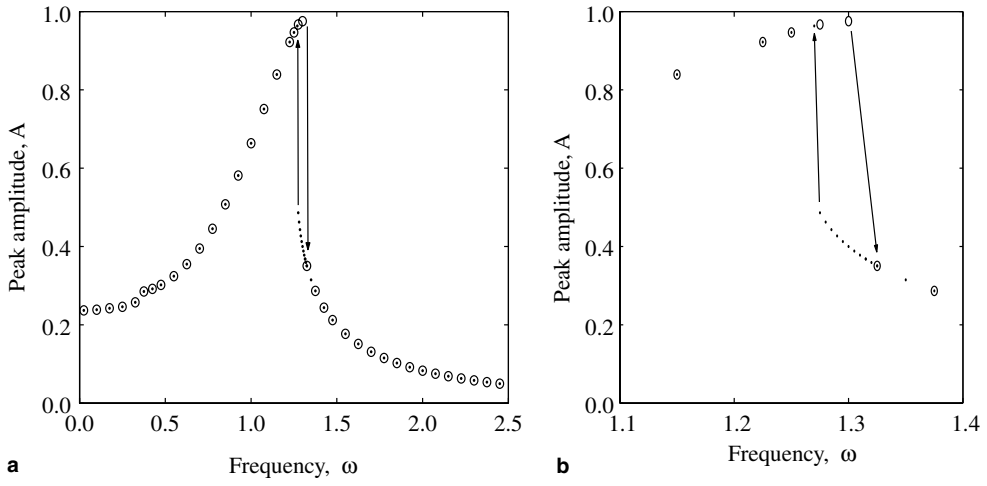

Fig. 2. Time marching results for $F = 0.25$. (a) For excitation frequency from 0 to 2.5. (b) A zoom-in picture of (a) for the hysteresis phenomenon. Open circle: increasing ω from 0.05; dot: decreasing ω from 2.50.

computed Duffing's equation solutions when using the standard harmonic balance method with one (HB1) and three harmonics (HB3). The results can be seen to be in excellent agreement with the time marching solutions. The one harmonic standard harmonic balance solution matches the time marching solution very well except for excitation frequencies near $\omega = 0.375$ where there is a slight increase in the solution peak amplitude. The HB3 solutions can be seen to further improve the solution accuracy by being able to model the region of slightly increased peak amplitude.

3.2.3. High dimensional harmonic balance results

We now discuss solutions computed via the high dimensional harmonic balance method (HDHB). We first note that all HDHB solutions are obtained using a Newton–Raphson (NR) procedure for Eq. (15). Thus an initial condition as the starting solution must be chosen. In generating the solution results shown in Fig. 2, for example, we sweep over the frequency range of interest. The HDHB method can yield different results depending on whether the solutions are obtained by an increasing or decreasing frequency sweep.

Figs. 4–6 show HDHB solutions for Duffing's equation when using one (HDHB1), two (HDHB2), and three harmonics (HDHB3), respectively, for the case where $F = 0.25$. Shown in the figures are the amplitudes for each harmonic used in each HDHB method, i.e. the zeroth and first harmonics for the HDHB1 method (Fig. 4), the zeroth, first, and second harmonics for HDHB2 method (Fig. 5), and the zeroth, first, second, and third harmonics for the HDHB3 method (Fig. 6). As mentioned previously, the high dimensional harmonic balance method has the ability to produce non-physical solutions. Whether or not the non-physical solutions are found depends on the initial condition solution chosen for the Newton–Raphson (NR) solver that is used to determine the HDHB solutions.

In Fig. 4, the HDHB solution results for the zeroth (A_0) and first (A_1) harmonic amplitudes are plotted as a function of the excitation frequency. Depending on whether one starts at an excitation frequency lower than the resonant frequency, or higher than the resonant frequency, two possible solution curves for each harmonic are possible. The pluses and stars shown in Fig. 4 are the computed zeroth and first harmonic amplitudes when starting at an excitation frequency of $\omega = 0.05$, and gradually increasing to a frequency of $\omega = 2.50$, at an incremental frequency step of $\omega = 0.05$. The squares and circles shown in Fig. 4 are the computed zeroth and first harmonic amplitudes when starting at an excitation frequency of $\omega = 2.50$, and gradually decreasing to a frequency of $\omega = 0.05$, also at an incremental frequency step of $\omega = 0.05$. As can be seen, when computing the HDHB1 solutions for increasing excitation frequencies, up to a frequency of approximately $\omega = 1.30$, the HDHB1 solution matches well the standard harmonic balance solution for both the zeroth and first harmonic components. However, beyond this frequency, the HDHB1 method produces

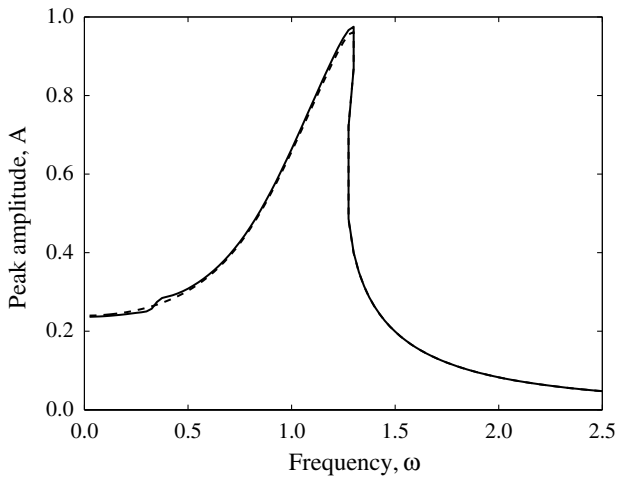

Fig. 3. HB results when one and three harmonics are included, for $F = 0.25$. Dash line: one harmonic; solid line: three harmonics.

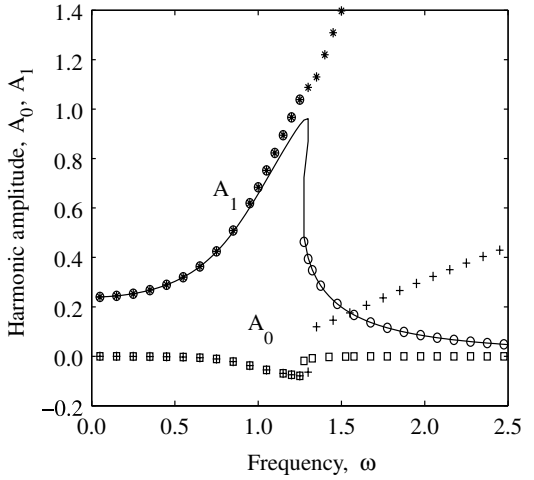

Fig. 4. The HDHB result when one harmonic is included, for $F = 0.25$, in comparison with the HB result with one harmonic. Star: A_1 by increasing ω; open circle: A_1 by decreasing ω; plus: A_0 by increasing ω; open square: A_0 by decreasing ω; solid line: the HB result.

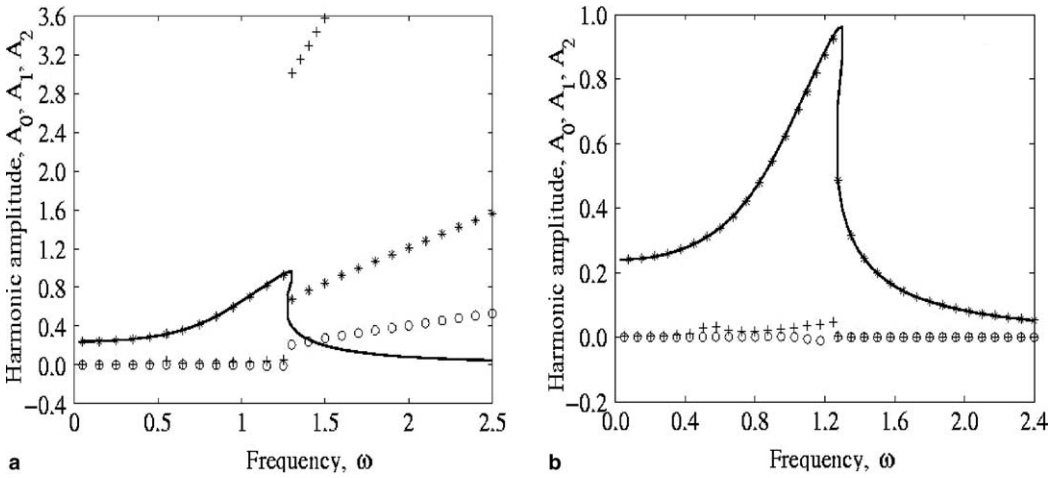

Fig. 5. The HDHB result when two harmonics are included, for $F = 0.25$, in comparison with the HB result with one harmonic. (a) Increasing ω from 0.05. (b) Decreasing ω from 2.4. Plus: A_2; star: A_1; open circle: A_0, solid line: HB result.

non-physical solutions as can be seen from the non-zero zeroth harmonic component and the further increasing of the first harmonic component.

The non-physical solution phenomenon can be seen more clearly in Fig. 5 for the HDHB2 results. In Fig. 5(a) and (b), the open circles, stars and pluses denote the HDHB2 results for the zeroth (A_0), first (A_1) and second harmonic amplitudes (A_2), respectively. Fig. 5(a) is for the results obtained by increasing the excitation frequency from $\omega = 0.05$, while Fig. 5(b) is for the results by decreasing the frequency from $\omega = 2.50$. There is an abrupt change in the amplitude responses near $\omega = 1.325$ in Fig. 5(a) and near $\omega = 1.270$ in Fig. 5(b). For the HDHB2 result found by increasing the frequency, A_2 and A_0 are near zero and A_1 matches HB1 result before the abrupt change. After the abrupt change, the first harmonic amplitude A_1 drops down slightly, while the zeroth and second harmonic amplitudes, A_0 and A_2, jump up. In particular, the value of A_2 is almost three times of A_1. These results are not physically meaningful solutions. The result found by decreasing the frequency matches well with the corresponding HB1 result with A_0 and A_2 near zero before and after the abrupt change.

For the results obtained by increasing the excitation frequency, the higher order HDHB analysis improves the amplitude response before the abrupt change. However, the non-physical response result after the abrupt

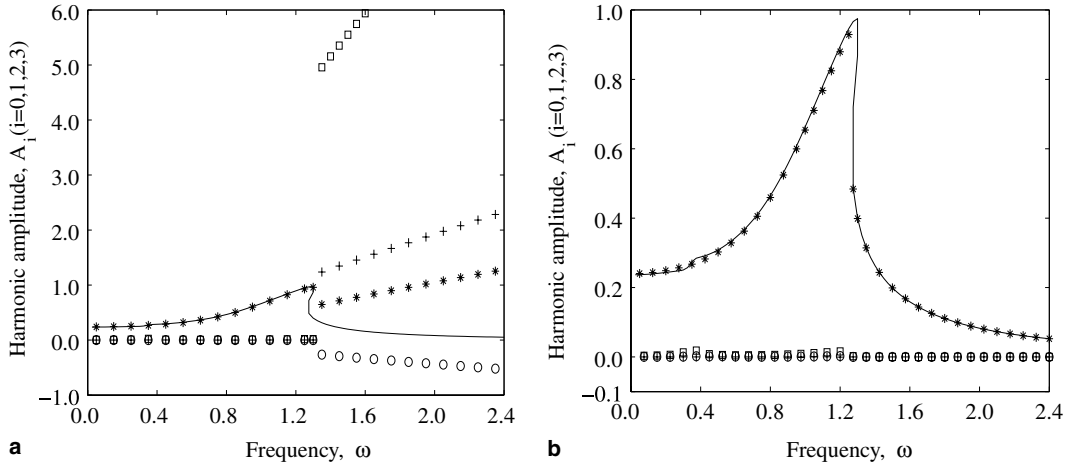

Fig. 6. The HDHB result when three harmonics are included, for $F = 0.25$, in comparison with the HB result with three harmonics. (a) Increasing ω from 0.05. (b) Decreasing ω from 2.4. Square: A_3; plus: A_2; star: A_1; open circle: A_0; solid line: HB result.

change is not improved and closer observation reveals that the result becomes even worse. Including more harmonics in the HDHB system improves the results obtained by decreasing the frequency, including the jump from low amplitudes to high amplitudes. Taking the HDHB3 result shown in Fig. 6 as an example, the result obtained by increasing the frequency matches the HB result well before the abrupt change (Fig. 6(a)). After the abrupt change, the amplitude of the third harmonic A_3 becomes four times that of A_2, A_2 is double that of A_1 and $A_0 < 0$ is nonzero. With large values in the amplitudes of the high harmonics, the Fourier series is divergent and these are non-physical solutions. The result found by decreasing the frequency is in an excellent agreement with the HB result (Fig. 6(b)).

Further insight can be obtained by comparing the HDHB results with the HB results for the peak amplitude responses as displayed in Fig. 7. The stars are for the HDHB results found by increasing the frequency, the open circles are for the HDHB results found by decreasing the frequency, while the solid lines are the HB results. To focus on the upper and lower branches of the amplitude-frequency curve, the non-physical solutions are not included in this figure. In Fig. 7(a), the HDHB1 and HB1 results are in excellent agreement for small and large values of frequency. A discrepancy between the HDHB1 and HB1 results is evident for $\omega \in [1.00, 1.380]$, and the two end points of the hysteresis are not clearly detected in the HDHB1 result. An improvement is seen in the HDHB2 result in Fig. 7(b), but the slight increase in the peak response amplitude near $\omega = 0.375$ is not predicted there. The HDHB3 result in Fig. 7(c) is identical to the HB3 result except for the unstable hysteresis branch that cannot be predicted in the HDHB system. The HDHB results with more harmonics are identical to the result in Fig. 7(c). By contrast the amplitudes of the higher harmonics for the non-physical solutions, i.e. the solutions found by increasing the frequency after the abrupt change near $\omega = 1.375$, become very large. These are not shown in Fig. 7. Further discussion about the non-physical solutions is presented in a later Section 3.4, including a rational way to distinguish between physical and non-physical solutions. The encouraging conclusion is that the HDHB method does accurately predict the physically correct solutions and that any non-physical solutions can be identified by the non-convergence of the Fourier series.

3.3. Strong nonlinearity with a large region of hysteresis

A large external force causes a great hysteresis. For $F = 1.25$, the region of the hysteresis is from $\omega = 1.75$ to $\omega = 2.40$, as shown in Fig. 8 for the time marching results and the HB results.

3.3.1. Time marching results

The time marching solutions for the peak response amplitude are shown in Fig. 8 as dots. The results are obtained by either gradually increasing the excitation frequency from 0.05 or gradually decreasing the

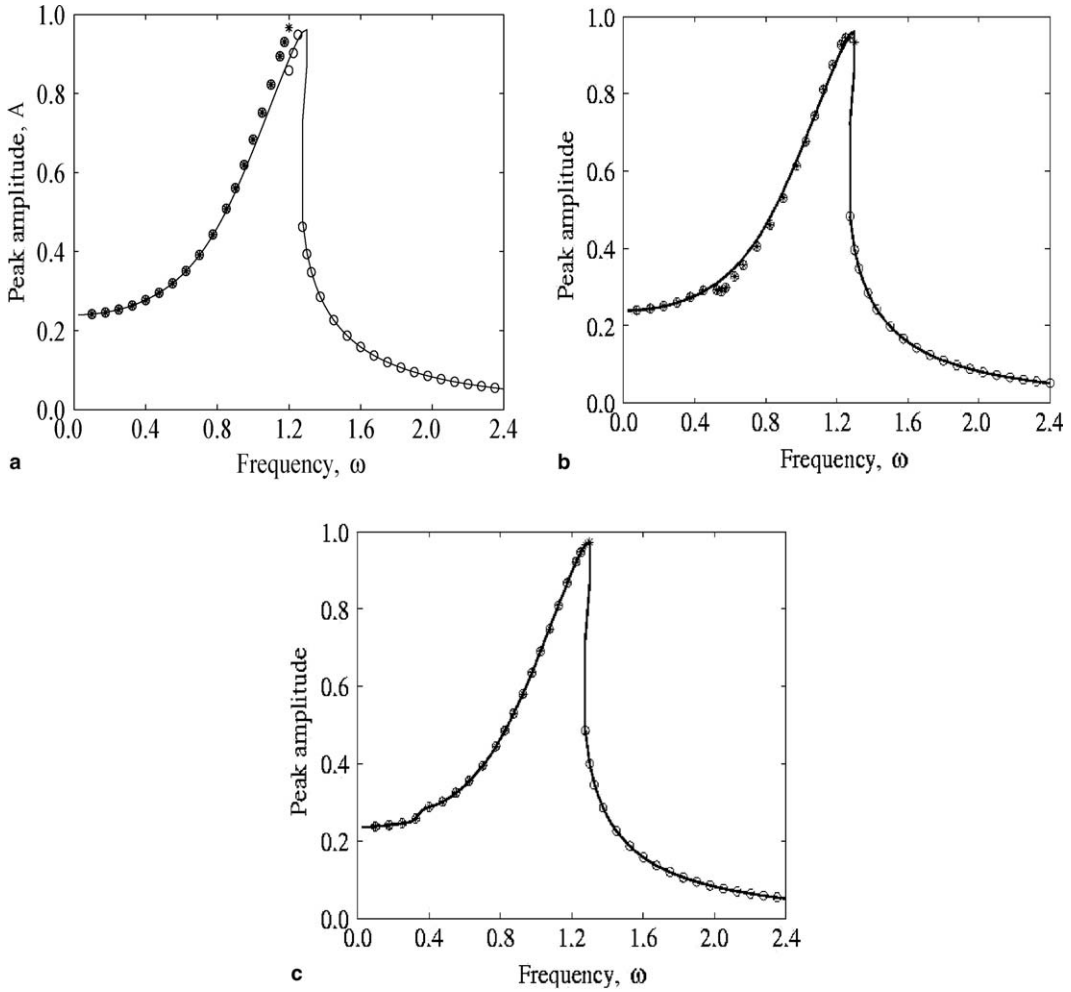

Fig. 7. The HDHB results with various number of harmonics, for $F = 0.25$, in comparison with the HB results. (a) One harmonic. (b) Two harmonics. (c) Three harmonics. Star: increasing ω from 0.05; open circle: decreasing ω from 2.4; solid line in (a) and (b): HB result with one harmonic; solid line in (c): HB result with three harmonics.

frequency from 2.80, while the previous oscillations are used as the initial condition in the solution process. When the frequency is increased, the motion amplitude increases gradually, but drops down rapidly from 2.50 to 0.25 near $\omega = 2.40$. On the other hand, when the frequency is decreased, the motion amplitude increases gradually, but jumps up from 0.50 to 2.00 near $\omega = 1.75$. Furthermore, when the frequency is near $\omega = 0.50$, the phenomenon of the slight increase in the peak amplitude becomes more evident and occurs more frequently than is the case when $F = 0.25$. Closer observation reveals that there are five to seven detectable harmonics in the motions near $\omega = 0.50$.

3.3.2. Harmonic balance results

The HB results in Fig. 8 are obtained by solving the simplified HB1 system for all possible solutions and then using lower order HB results as initial points in the NR process for higher order HB results. The HB solutions for the zeroth and eventh harmonics amplitudes are nearly zero. Typical results for HB1, HB3 and HB5, are presented in Fig. 8. The HB5 result is in an excellent agreement with the time marching result. Higher order HB results do not improve much upon the HB5 result as the amplitudes for the higher harmonics are nearly zero. The unstable and lower branches of the HB1, HB3 and HB5 coincide, and the prediction for the lower branch matches well with the time marching result. For the upper branch when ω is from 1.0 to 2.5,

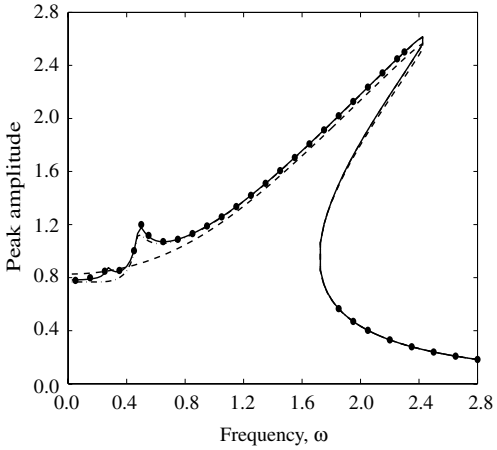

Fig. 8. Comparison of the results from the time marching and the HB methods, $F = 1.25$. Dot: time marching; dash line: HB result with one harmonic; dash dot line: HB result with three harmonics; solid line: HB result with five harmonics.

the HB1 result is slightly lower than the time marching result, while the HB3 and HB5 results are in an excellent agreement with the time marching results. The significant improvement of higher order HB upon lower order HB results is seen at the slight increase of the peak response amplitude near $\omega = 0.50$ where many high harmonics are present. The HB1 curve for the peak response amplitude increases smoothly and no slight increase occurs near $\omega = 0.50$. The HB3 curve detects one local peak amplitude at $\omega = 0.50$, and the HB5 curve captures two such peaks. The chosen increment for the frequency in Fig. 8 is $\Delta\omega = 0.05$. With a finer $\Delta\omega$, more local peaks may be detected.

3.3.3. High dimensional harmonic balance results

Some typical results for the HDHB with different numbers of harmonics are shown in Figs. 9–11. The results are obtained by increasing/decreasing the frequency and using previous results as the initial starting points in the solution process.

Fig. 9 shows the HDHB results when one harmonic is included in the analysis, in comparison with the HB1 results. The results by increasing the frequency are denoted by stars, and the results by decreasing the frequency are denoted by open circles. An interesting observation is that there is no rapid change in the motion amplitudes when the frequency is increased gradually, while the jump (near $\omega = 1.75$) from low amplitudes to high amplitudes is captured by the solution response when the frequency is decreased.

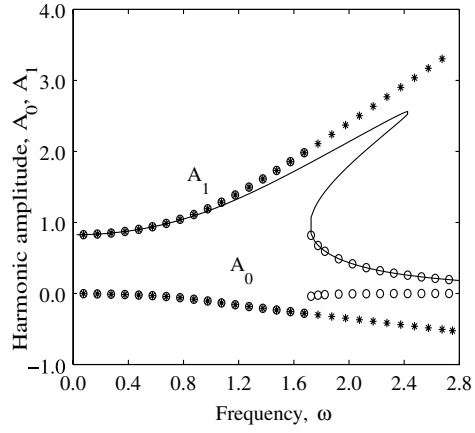

Fig. 9. HDHB results with one harmonic, $F = 1.25$. Star: A_1 by increasing ω from 0.05; open circle: A_1 by decreasing ω from 2.75; solid line: HB result with one harmonic.

The HDHB2 results, i.e. the HDHB results when two harmonics are included in the analysis, are shown in Fig. 10, in comparison with the HB1 results denoted by a solid line. Fig. 10(a) is for the results obtained by increasing the frequency, while Fig. 10(b) is for the results obtained by decreasing the frequency. In both figures, the amplitudes of the zeroth A_0, the first A_1 and the second A_2 harmonic are denoted by open circles, stars and pluses respectively. The HDHB results found by increasing the frequency match the upper branch of the HB1 result well for frequencies up to 0.75, after which the HDHB solutions deviate from the HB1 motions. The HDHB results found by decreasing the frequency match the lower and upper branches of the HB1 results well except for frequencies between 0.75 and 1.75, when the HDHB solutions are larger than the HB1 solutions. These HDHB2 solutions are non-physical solutions because the amplitude of the second harmonic is much larger than that of the first harmonic. The increment used for the frequency in Fig. 10 is 0.05, which is sufficiently small for the cases discussed so far. Decreasing the frequency increment to 0.0001 does not improve the HDHB2 results.

When three and four harmonics are included in the HDHB analysis, the NR solver never converges for frequencies near 0.75, therefore, a complete set of the HDHB3 and HDHB4 results cannot be obtained. This phenomenon occurs when the frequency is increased from 0.05 or decreased from 2.80.

However, the HDHB results are improved and the above phenomenon disappears when more harmonics are included in the analysis. If a sufficiently small $\Delta\omega$ is used, the NR solver converges when more than five harmonics are included in the HDHB system. Some examples are: the NR converges for HDHB5 with $\Delta\omega < 0.001$, while it converges for HDHB6, HDHB7 and HDHB8 with $\Delta\omega < 0.025$. The higher order HDHB results are in good agreement with the upper and lower branches of the lower order HB results. For example, the HDHB5 and HDHB6 results are close to the HB3 results; while the HDHB7 and HDHB8 solutions are close to the HB5 solutions. A typical result is shown in Fig. 11 for the HDHB8 solutions, in comparison with the HB5 result. The accumulated amplitude is used in this figure. The HDHB8 result obtained by increasing the frequency follows the upper branch of the HB5 result till $\omega = 2.45$, after which the HDHB solution jumps up to 20 and never drops down to the lower branch. The HDHB8 result obtained by decreasing the frequency is identical to the HB5 result, including the lower and upper branches, and the jump near $\omega = 1.75$. The encouraging conclusion is that with a large enough number of harmonics, HDHB works well even when siginificant amounts of mysteresis occur.

3.3.4. Unstable solutions

It should be noted that the HDHB results presented in the above are not capable of predicting the solutions between the upper and lower branches of the hysteresis, e.g. the peak amplitude 2.0 for the frequency 2.1, while these unstable solutions are captured by the HB results. It should also be noted that the procedure used

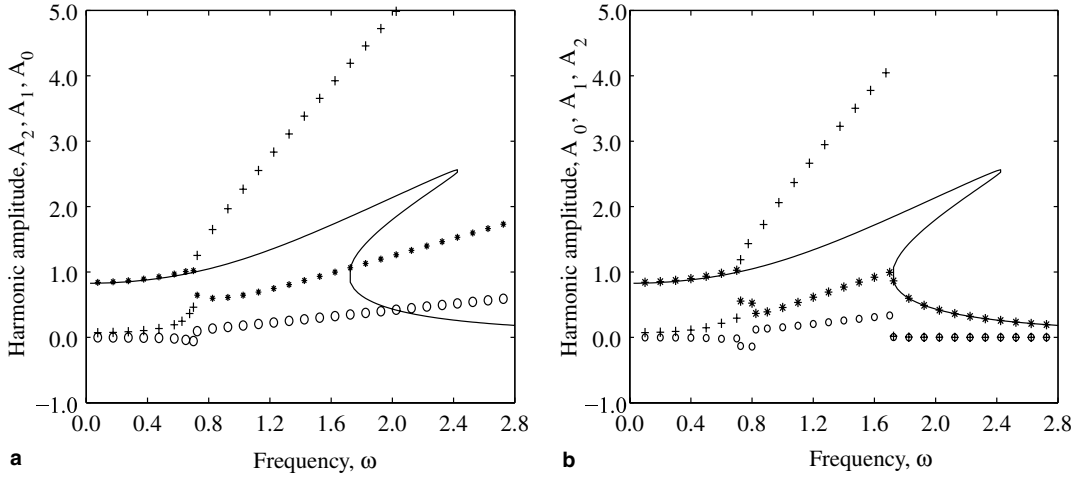

Fig. 10. HDHB results with two harmonics, $\Delta\omega = 0.05$, $F = 1.25$. (a) Increasing ω from 0.05. (b) Decreasing ω from 2.75. Plus: A_2; star: A_1; open circle: A_0; solid line: HB result with one harmonic.

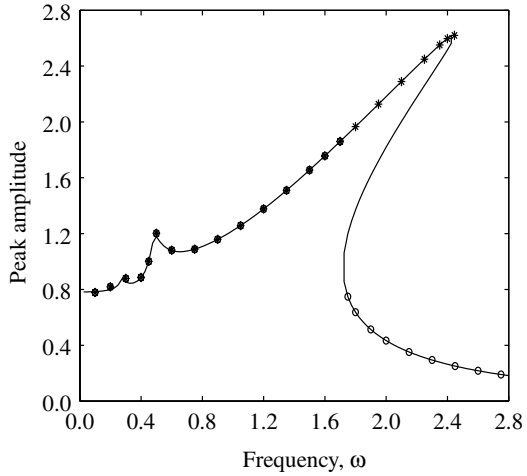

Fig. 11. HDHB results with eight harmonics, $\Delta\omega = 0.0005$, $F = 1.25$. Star: increasing ω from 0.05; open circle: decreasing ω from 2.75; solid line: HB result with five harmonics.

to determine the HDHB solutions is either to increase or decrease the frequency while using the previous results as the initial condition in the NR solver. This solution process usually misses the unstable branch of the hysteresis. For example, using this procedure for the HB system one also cannot detect the unstable branch. However, using an alternate approach in solving the HDHB system does provide the results for the unstable branch, as described next.

For the results shown before, the force F and frequency ω are given, and the amplitudes are computed from the HDHB systems. Another way to solve the system is to fix the force F, prescribe A_1 and solve the system for ω and other amplitudes, e.g. A_0 and A_2. Fig. 12 is for the HDHB1 result obtained by increasing A_1 and using the previous result as initial guess in the NR solver. If the first prescribed A_1 is near 0.9, the HDHB1 prediction follows the upper branch of the response curve. If the first prescribed A_1 is near 0.1, the HDHB1 prediction follows the lower branch of the response curve, then continuously follows the unstable branch. Both curves do not detect any abrupt change near $\omega = 2.45$ and increase gradually as the value of A_1 increases. In the above procedure, the unstable branch of the hysteresis is captured in the HDHB system, while the two end points of the hysteresis cannot be detected as there is no abrupt change in the predicted curves.

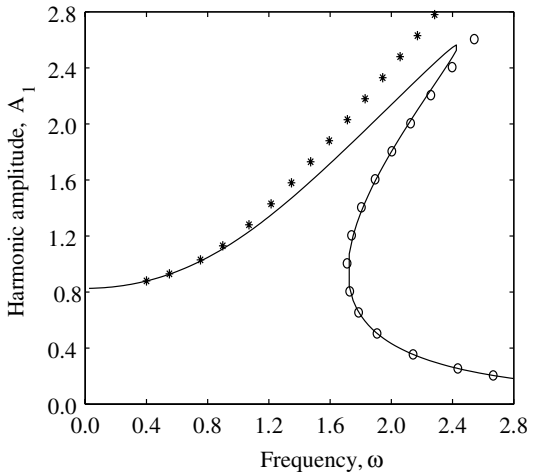

Fig. 12. HDHB results with one harmonic, $F = 1.25$. Star: increasing A_1 from 0.76; open circle: increasing A_1 from 0.15; solid line: HB result with one harmonic.

3.4. Non-physical solutions

Generally speaking, the HDHB method provides more solutions than the HB method and the time marching scheme. Most (perhaps all) of the additional solutions are non-physical solutions. This subsection presents a further investigation on these solutions.

From the preceding discussion, the HDHB peak amplitude solutions obtained by increasing the frequency never drop down to the small amplitude motions, instead the solutions jump up and keep increasing as the frequency is increased. The HDHB predicted motions after the jump are non-physical solutions.

These non-physical solutions can be identified by the non-convergence of the Fourier series. For example, from Section 3.2, the multi-solutions including non-physical solutions occur for the external frequencies beyond the hysteresis interval, i.e. $\omega > 1.375$. Using different initial guesses in the N-R solver, one may obtain the physical solution with a small peak amplitude and the non-physical solutions with large peak amplitudes. For $\omega = 1.4$, a physical solution is obtained and shown in Table 1 when the initial guess is taken to be zero; a non-physical solution is obtained and shown in Table 2 when the initial guess is taken to be 10. The two tables display the solutions for the amplitudes of the harmonics for harmonic numbers from 1 to 5. In both tables, for the purpuse of simplification, we use the notation of $C(n)$ for the coefficient of $\cos(n\omega t)$ and $S(n)$ for the coefficient of $\sin(n\omega t)$. From the first row of data in Table 1, as the number of harmonics increases, it is seen that the coefficients of $\cos(\omega t)$ and $\sin(\omega t)$ converge to -0.077527 and -0.25141, respectively. The amplitude of the second harmonic approaches zero when the number of harmonics becomes large, and so does the amplitude of the fourth harmonic. The coefficients of $\cos(3\omega t)$ and $\sin(3\omega t)$ are fixed at 2.2×10^{-4} and 1.6×10^{-4}, respectively. Therefore, it is reasonable to conclude that the solution of the motion converges to

$$x(t) = -0.077527\cos(1.4t) - 0.25141\sin(1.4t) + 2.2 \times 10^{-4}\cos(4.2t) + 1.6 \times 10^{-4}\sin(4.2t) + (\text{h.o.t.}). \tag{28}$$

The Fourier series for the above motion converges since the amplitude of the harmonic decreases as the order of harmonic increases. The peak amplitude of the above motion converges to 0.2 as the number of harmonics approaches infinity. From Table 2, on the other hand, there is no convergence in the harmonic amplitudes. From the rows of data in the table, it is seen that there is no obvious convergence for the coefficients of $\cos(n\omega t)$ or $\sin(n\omega t)$. From the columns, it is seen that the harmonic amplitude increases as the order of harmonic increases, indicating that the Fourier series diverges, e.g., in column $N_H = 5$, $S(1) < S(2) < S(3) < S(4) < S(5)$. Furthermore, the peak amplitude of the solution increases as the number of harmonics increases. This is further explored in the following discussion.

The amplitudes for the motions near the jump displayed in Fig. 13(a) are from the HDHB method when various number of harmonics are included in the analysis. Before the jump, the results from the HDHB method are identical to the results from the HB method and the time marching scheme; after the jump, the more harmonics included in the HDHB system, the larger the motions amplitudes become. The relationship between the number of harmonics and the amplitude of the motion right after the jump are shown in

Table 1
The convergence of a physical solution

	$N_H = 1$	$N_H = 2$	$N_H = 3$	$N_H = 4$	$N_H = 5$
C(1)	-7.7174×10^{-2}	-7.7538×10^{-2}	-7.7527×10^{-2}	-7.7527×10^{-2}	-7.7527×10^{-2}
S(1)	-2.5120×10^{-1}	-2.5144×10^{-1}	-2.5141×10^{-1}	-2.5141×10^{-1}	-2.5141×10^{-1}
C(2)		4.8968×10^{-4}	-2.1008×10^{-6}	5.1544×10^{-9}	-5.7242×10^{-12}
S(2)		4.6208×10^{-4}	2.2565×10^{-7}	2.7321×10^{-9}	-1.1988×10^{-11}
C(3)			2.2336×10^{-4}	2.2336×10^{-4}	2.2336×10^{-4}
S(3)			1.6038×10^{-4}	1.6038×10^{-4}	1.6038×10^{-4}
C(4)				-4.7110×10^{-7}	8.4266×10^{-10}
S(4)				2.8979×10^{-8}	5.4799×10^{-10}
C(5)					-2.9823×10^{-7}
S(5)					-1.4280×10^{-9}

Table 2
The non-convergence of a non-physical solution

	$N_H = 1$	$N_H = 2$	$N_H = 3$	$N_H = 4$	$N_H = 5$
C(1)	−0.8898	−0.5219	−0.6433	0.3630	0.6283
S(1)	0.9126	−0.5082	0.2570	−0.5584	0.2105
C(2)		−0.6545	−0.9054	−0.4125	0.6760
S(2)		−3.2173	0.9281	−0.8669	0.4944
C(3)			−1.4560	−1.8470	0.7581
S(3)			4.9458	−0.1423	1.0074
C(4)				−3.7511	0.8730
S(4)				5.8848	2.2594
C(5)					0.9609
S(5)					8.7322

Fig. 13(b), where the reciprocal of the peak amplitude, $1/A$, is plotted versus the reciprocal of the number of harmonics retained in the computation, $1/N_H$. This is so the asymptotic behavior is more readily observed, i.e. $A \to \infty$ or $1/A \to 0$ as $N_H \to \infty$ or $1/N_H \to 0$. The time marching and HB results for the amplitude at the turning point $\omega = 1.315$ is near $A = 0.95$ or $1/A \approx 1.0$. The amplitude predicted from the HDHB system when one harmonic is included is not far away from 0.95, while the amplitude from the HDHB system when many harmonics are included increases dramatically as the number of the harmonics increases. More higher order HDHB results are included in Fig. 13(b), e.g. the results when 20 harmonics and 40 harmonics are included. This figure shows that the amplitude of the non-physical solutions are pushed away to infinity when sufficient harmonics are included in the HDHB analysis. The results for case $F = 1.25$ are similar to those of Fig. 13, which are for case $F = 0.25$.

Fig. 12 shows that the unstable branch of the hysteresis can be captured by the HDHB analysis. In addition, in the hysteresis region, various initial starting points in the NR iteration may lead to results other than those from the HB prediction. These additional solutions are also non-physical solutions. In order to capture these HDHB solutions, another procedure is employed to solve the nonlinear HDHB system.

The results in Figs. 14–16 and the "cross" in Fig. 17 are obtained by the following procedure: fix the value of the frequency, prescribe the amplitude of the first harmonic A_1, and solve the system for the external force F

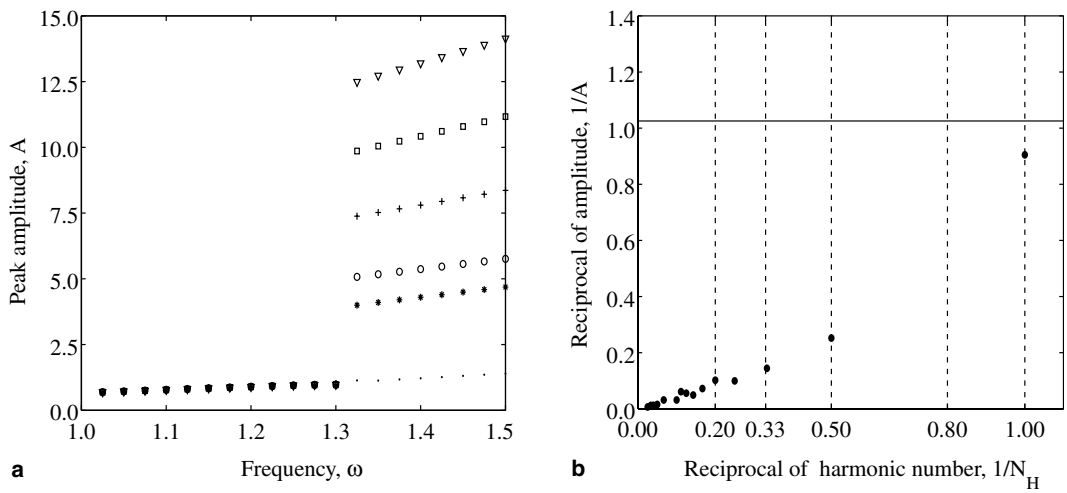

Fig. 13. The HDHB solution amplitudes at the turning points for various numbers of harmonics N_H, $F = 0.25$: (a) Peak amplitude versus the frequency. Dot: $N_H = 1$; star: $N_H = 2$; open circle: $N_H = 3$; plus: $N_H = 4$; open square: $N_H = 5$; open triangle: $N_H = 6$. (b) The reciprocal of amplitude versus the reciprocal of the number of harmonics. Solid line: the amplitude value at the turning point from the marching and HB methods; dot: results for HDHB with various number of harmonics.

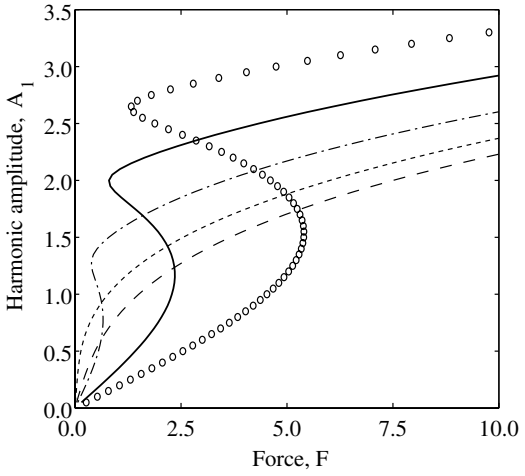

Fig. 14. HB results with one harmonic for various frequency. Dash line: $\omega = 0.5$; dot line: $\omega = 1$; dash dot line: $\omega = 1.5$; solid line: $\omega = 2$; open circle: $\omega = 2.5$.

and the other amplitudes. In this way, the HB1 result is easy to obtain when the simplified Eq. (11) is used. For a prescribed A_1, there is a unique solution for F, which is calculated by (11). The HB1 results for various ω are reported in Fig. 14. From this figure of the amplitude-force relationship, for large driving frequency ($\omega \geqslant 3$), multi-solutions of the response amplitudes exist for certain external forces, i.e. the hysteresis phenomenon occurs. For example, when $\omega = 2.50$, the amplitude increases when the force increases gradually, but then at F near 22.5, A_1 jumps up from 1.5 to 3. Conversely, A_1 decreases when F decreases gradually, but then at F near 1.25, A_1 drops dramatically from 2.5 to 0.25. Furthermore, the larger the driving frequency is, the larger the region of hysteresis is.

The HDHB system becomes easy to solve when the frequency is given and the amplitude of the first harmonic is prescribed. A Maple program is able to obtain all possible solutions from the HDHB1 system, and the results are displayed in Fig. 15, in comparison with the the corresponding HB1 results. For small frequencies, the HDHB1 results are close to the HB1 results. The discrepancy between the HDHB1 and HB1 results becomes significant when the hysteresis occurs, e.g. $\omega = 1.5$. Unlike the HB1 result where the solution for the force F is unique for a prescribed amplitude of the first harmonic A_1, the HDHB1 solutions for F can

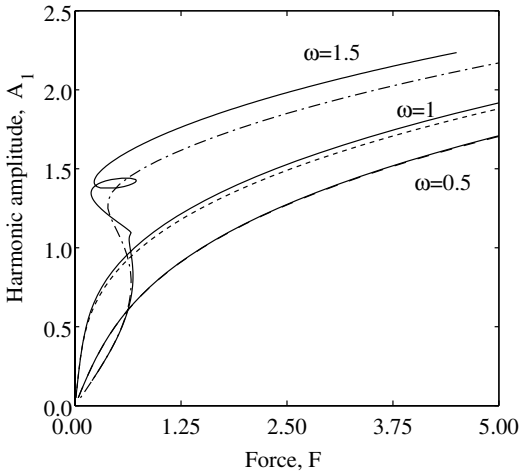

Fig. 15. The HDHB results with one harmonic, in comparison with the corresponding HB results. Dash line: $\omega = 0.5$; dot line: $\omega = 1$; dash dot line: $\omega = 1.5$; solid line: HDHB results.

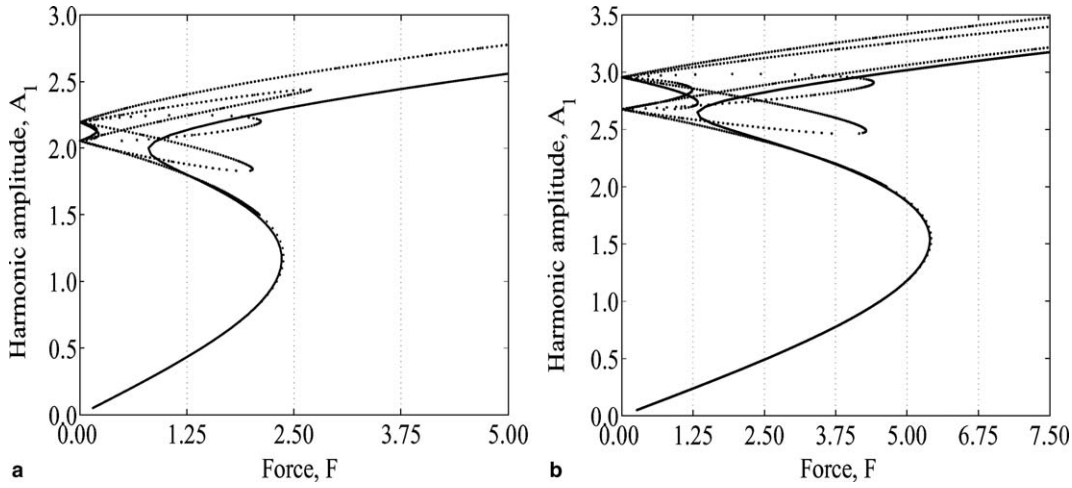

Fig. 16. Comparison of the HDHB and HB results with one harmonic. (a) For $\omega = 2.0$. (b) For $\omega = 2.5$. Dot: HDHB results; solid line: HB results.

be multiple valued. The HDHB1 curve for $\omega = 1.5$ is twisted as a small loop near the small hysteresis region predicted by the HB1 system. The HDHB1 results are identical to the HB1 results for small amplitudes ($A_1 \leqslant 1.5$). This phenomenon is further verified in Fig. 16 for $\omega = 2$ and $\omega = 2.5$.

Fig. 16(a) presents the HDHB1 result for $\omega = 2$, in comparison with the HB1 result. For A_1 between 1.5 and 2.5, there are many solutions for F. In the hysteresis region, for F between 3 and 9, there are as many as nine different response amplitudes for a fixed force. Among these solutions, two are on the lower and unstable branches of the HB1 result, and one is close to the upper branch of the HB1 curve. The turning point from the upper branch to the lower branch cannot be detected in the HDHB1 curve, while the lower and unstable branches of the HB1 result are predicted accurately in the HDHB1 approach.

A similar phenomenon can be found in Fig. 16(b) for the HDHB1 result for $\omega = 2.5$. In the hysteresis region for F between 1.25 and 22.5, there are also as many as nine solutions, among which three match well with the HB1 solutions. The lower branch, the turning point from the lower to the upper branches and the unstable branch are predicted in the HDHB1 with a fairly good accuracy.

However, the branch in the HDHB1 result that is close to the upper branch of the HB1 result cannot be captured by using the procedures in Sections 3.2 and 3.3. In fact, after the jump, the motion jumps up to the top branches of the HDHB1 curves in Fig. 16.

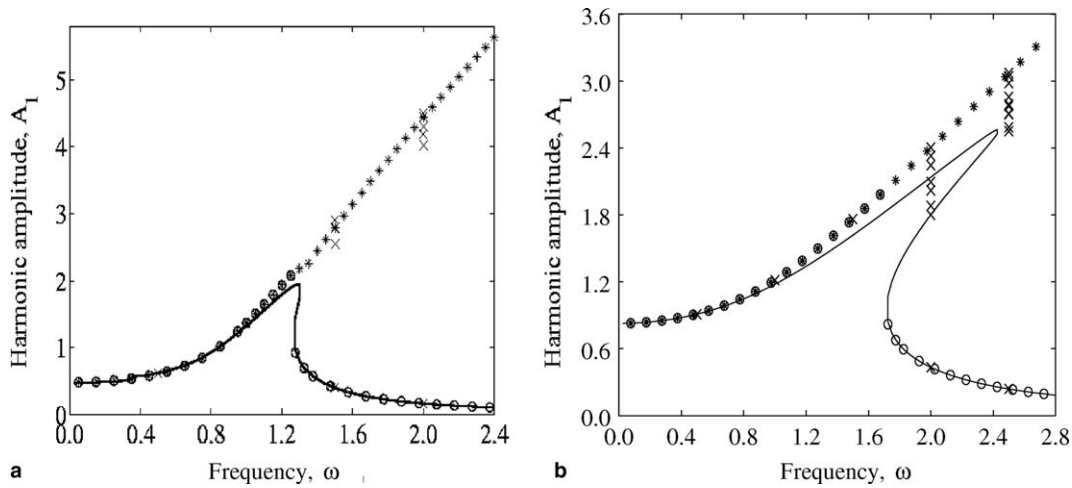

Fig. 17. Non-physical solutions of HDHB results with one harmonic, in comparison with the HB result with one harmonic. (a) $F = 0.25$. (b) $F = 1.25$. Star: increasing ω from 0.05; open circle: decreasing ω from 2.75; cross: cross plot from Figs. 14–16; solid line: HB result.

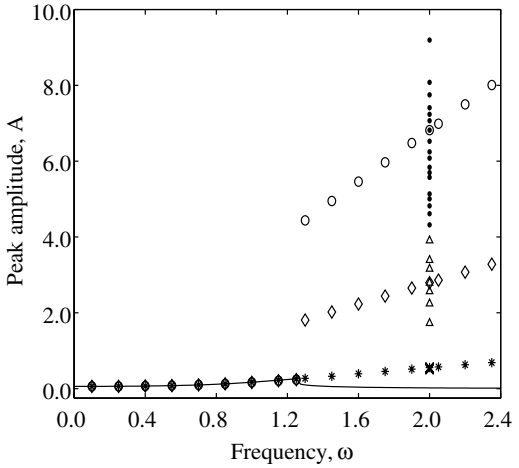

Fig. 18. Non-physical solutions from higher order HDHB systems for $F = 1.25$. Star and cross: HDHB results with one harmonic; diamond and triangle: HDHB results with four harmonics; open circle and dot: HDHB results with eight harmonics.

For large excitation frequencies, besides the solutions that are near the HB1 solutions, there are additional solutions from the HDHB1 system. To further investigate these additional solutions, the HDHB results in Fig. 16 are added into the figures of amplitude versus frequency by cross plotting. Fig. 17(a) shows that the additional solutions in the amplitude versus the frequency plot for $F = 0.25$, and Fig. 17(b) is for $F = 1.25$. From these two figures, the additional solutions are clustered near the upper branch. These solutions start to appear when the hysteresis starts ($\omega = 1.25$ in Fig. 17(a) and $\omega = 1.75$ in Fig. 17(b)), and they remain for larger frequencies, never to disappear.

In order to further investigate the non-physical solutions from the higher order HDHB systems, various initial conditions are used for the NR solver. The results from HDHB4 and HDHB8 are chosen to display in Fig. 18 together with the HDHB1 result from Fig. 17(a). The vertical axis is for the peak amplitude, i.e. the highest peak in the solution motion. The diamonds are the HDHB4 results found by increasing the frequency and using the previous result as the initial condition for the NR solver. Similarly, the open circles are the HDHB8 results found by increasing the frequency. Various non-physical solutions are further investigated for $\omega = 2$. From the HDHB4 system, various initial conditions are used in the NR iteration, and seven distinct solutions are obtained shown as triangles in Fig. 18. A random number generator is used for the initial condition, and the values vary from -10 to 10. Thousands of sets of random initial values are used to generate the results shown in Fig. 18. The probability for converging to the solution with the largest peak near 3 is close to 45%, and the probability for converging to the solution on the upper branch near 2 is about 40%. The other solutions have a much smaller probability. The solution on the lower branch is very hard to capture if the initial condition values are randomly chosen. Furthermore, when the initial guess for the NR is near zero, the NR procedure may not converge. The HDHB8 results shown as dots in the figure show the same phenomenon. There are 18 detected distinct solutions near the solution on the upper branch, ranging from 3 to 9. The probability for the solution on the lower branch is essentially zero, the highest solution (near 9) has the largest probability of 45%, and the second largest probability 40% occurs for the solution on the upper branch. This phenomenon remains for other frequencies and higher order HDHB systems. This demonstrates that the non-physical solutions are pushed toward infinity in the higher order HDHB systems.

4. Conclusion

It is demonstrated using the Duffing's oscillator as a prototypical system that the difference between the HB and HDHB systems are from the nonlinear terms in the original system. From the analytical expressions derived for the HB and HDHB systems, it is shown that there are additional terms in the HDHB system. The advantages and disadvantages of both HB and HDHB methods, as drawn from the numerical simulations

in this study, are summarized as follows. The HB results provide high accuracy. There are no non-physical solutions (divergent Fourier series) found from the HB analysis. The number of harmonics retained in the HB procedure usually is smaller, compared to that included in the HDHB method for the same accuracy of the results. However, when many high harmonics are included in the HB method, the analytical HB system becomes extremely complex and time consuming. For the HDHB method, accurate results can be obtained for all physically meaningfully solutions by using a large number of the harmonics in the analysis. However, there are non-physical solutions in the HDHB method as well, in particular, for the motions near/in the hysteresis region. These non-physical solutions may be identified by the non-convergence of the Fourier series. On the other hand, the HDHB system is easy to derive and implement into a computer program regardless of the number of harmonics included in the analysis and non-smooth nonlinearities may be treated in a straightforward manner. For small to moderate amplitude motions, the HDHB and HB results are close to each other. For larger motions, especially those near the hysteresis region, the discrepancy between the HDHB and HB results may become significant for a fixed number of harmonics. The result from the classical HB approach is more accurate than the HDHB approach with the same number of harmonics included in the analysis. In order to obtain the same order accuracy from the HDHB method, almost twice the number of harmonics must be retained in the analysis compared to those needed in the HB analysis.

Acknowledgment

The author Liu thanks for the support from NSERC (Natural Sciences and Engineering Research Council) of Canada.

References

[1] L.N. Virgin, On the harmonic response of an oscillator with unsymmetric restoring force, J. Sound Vib. 126 (1) (1988) 157.
[2] S.F. Shen, An approximate analysis of nonlinear flutter problems, J. Aerosp. Sci. 26 (1) (1959) 25.
[3] S.J. Price, H. Alighanbari, B.H.K. Lee, The aeroelastic response of a two-dimensional airfoil with bilinear and cubic structural nonlinearities, J. Fluids Struct. 9 (1995) 175.
[4] D. Tang, E.H. Dowell, L.N. Virgin, Limit cycle behaviour of an airfoil with a control surface, J. Fluids Struct. 12 (1998) 839.
[5] L.C. Zhao, Z.C. Yang, Chaotic motions of an airfoil with nonlinear stiffness in incompressible flow, J. Sound Vib. 138 (1990) 245.
[6] P. Donescu, L.N. Virgin, J.J. Wu, Periodic solutions of an unsymmetric oscillator including a comprehensive study of their stability characteristics, J. Sound Vib. 192 (5) (1996) 959.
[7] L. Liu, E.H. Dowell, The secondary bifurcation of an aeroelastic airfoil motion: effect of high harmonics, Nonl. Dyn. 37 (1) (2004) 31.
[8] L. Liu, E.H. Dowell, High harmonic balance approach for an airfoil with a freeplay control surface, AIAA J. 43 (4) (2005) 802.
[9] J.P. Thomas, E.H. Dowell, K.C. Hall, Nonlinear inviscid aerodynamic effects on transonic divergence, flutter, and limit-cycle oscillations, AIAA J. 40 (4) (2002) 638.
[10] K.C. Hall, J.P. Thomas, W.S. Clark, Computation of unsteady nonlinear flows in cascades using a harmonic balance technique, AIAA J. 40 (5) (2002) 879.
[11] S.P. Beran, C.L. Pettit, A direct method for quantifying limit-cycle oscillation response characteristics in the presence of uncertainties, AIAA Paper 2004-1695, 2004.
[12] Y.B. Kim, S.T. Noah, Y.S. Choi, Periodic response of multi-disk rotors with bearing clearances, J. Sound Vib. 144 (3) (1991) 381.
[13] M. McMullen, A. Jameson, J.J. Alonso, Acceleration of convergence to a periodic steady state in turbomachinery flows, AIAA Paper 2001-0152 2001.
[14] M. McMullen, The application of non-linear frequency domain methods to the Euler and Navier–Stokes equations, PhD dissertation, Stanford University, 2003.
[15] L.N. Virgin, Introduction to Experimental Nonlinear Dynamics, Cambridge University Press, Cambridge, 2000.
[16] R. Seydel, Practical Bifurcation and Stability Analysis: From Equilibrium to Chaos, Springer-Verlag, New York, 1994.